Scripta Materialia 264 (2025) 116720

Contents lists available at ScienceDirect

Scripta Materialia

journal homepage: www.journals.elsevier.com/scripta-materialia

Continuously adjustable metal to insulator transitions within high temperature range for $La_{3-x}Bi_xNi_2O_7$ layered perovskite nickelates

Hao Zhang [a], Jingxin Gao [a], Yi Bian [a], Wei Lei [a], Hongliang Dong [b,c,d], Xiaoguang Xu [a], Nuofu Chen [e], Jikun Chen [a,*]

[a] School of Materials Science and Engineering, University of Science and Technology Beijing, Beijing 100083, China
[b] Center for High Pressure Science and Technology Advanced Research, Shanghai 201203, China
[c] Shanghai Key Laboratory of Material Frontiers Research in Extreme Environments (MFree), Shanghai Advanced Research in Physical Sciences (SHARPS), Shanghai 201203, China
[d] State Key Laboratory of High Performance Ceramics and Superfine Microstructure, Shanghai Institute of Ceramics, Chinese Academy of Sciences, Shanghai 201899, China
[e] School of Renewable Energy, North China Electric Power University, Beijing 102206, China

ARTICLE INFO

Keywords:
Ruddlesden-Popper type layered perovskite
Rare-earth nickelates
Metal to insulator transition
Material stability

ABSTRACT

Establishing the Ruddlesden-Popper type layered perovskite structures for rare-earth nickelates (e.g., $Re_{n+1}Ni_nO_{3n+1}$), by alternatively inserting one *Re*O rock-salt layer into n layers of the *Re*NiO_3 perovskite, sheds a light on new freedom to regulate their metal to insulator transition (MIT) properties. Herein, we demonstrate continuously regulatable MITs enabling significantly enhanced resistive switches at high temperature range of 500–560 K for $La_{3-x}Bi_xNi_2O_7$ (n=3), compared to conventional *Re*NiO_3 with similar critical temperatures (T_{MIT}). Anomalously small magnitudes in thermopowers are observed for the insulating $La_{3-x}Bi_xNi_2O_7$, compared to the 113-type nickelates, indicating their distinguished bi-polar transport characters. The Bi substitution results in electron localization as indicated by the near edge X-ray absorption fine structure analysis, and elevates the hole contribution to the transportation to drive the thermopower associated with their insulating phase towards positive magnitudes. Furthermore, compared to *Re*NiO_3, the $La_{3-x}Bi_xNi_2O_7$ exhibits higher material stability, paving the way to their applications.

The electron correlations within D-band transitional metal oxides, such as the family of perovskite nickelates, enables distinguished metal to insulator transitions (MIT) beyond conventional semiconductors [1]. As a representative case, the *Re*NiO_3 experiences reversable charge disproportionation, e.g., $Ni^{3+}(t_{2g}^6e_g^1)\rightarrow Ni^{(3\pm\delta)}(t_{2g}^6e_g^{1\pm\delta})$, when descending (or elevating) temperature across a critical point (T_{MIT}) [2–4]. This results in abrupt variation in the electrical and optical properties that is useful in potential applications such as critical temperature resistive (CTR) thermistor [5], correlated electronic devices [6,7], thermochromic and infrared camouflage [8]. The *Re*NiO_3 easily achieves a widely adjustable T_{MIT} ranging from 100–600 K by altering its rare-earth composition [9]. For example, enlarging the rare-earth ionic radius straighten the Ni-O-Ni bond that narrows the energy band gap split from the upper Hubbard band (UHB, conduction band) of Ni-3d and O-2p (valance band) and therefore descend T_{MIT} [10–12]. Furthermore, the *Re*NiO_3 exhibits high material stability in air and even sea water, and this paves the way to their practical device applications [13]. Nevertheless, the resistive switch across MIT ($R_{Insul.}/R_{Met.}$) of *Re*NiO_3 decreases as T_{MIT} increases, resulting in a less abrupt MIT behavior at high temperatures (above 400 K) for compositions after Sm [14], and this impedes the potential applications of *Re*NiO_3 at high temperature ranges.

Establishing the Ruddlesden-Popper type layered perovskite structures (e.g., $Re_{n+1}Ni_nO_{3n+1}$) sheds a light to further improve the abruption in MIT behaviors for the perovskite family of nickelates that extends their applications towards higher range of temperatures [15,16]. The structure of $Re_{n+1}Ni_nO_{3n+1}$ can be seen as to insert one layer of *Re*O rock-salt structure within n layers of *Re*NiO_3 perovskite structure [17–19]. This results in confinements of the carrier transportation along the NiO_6 octahedra within the perovskite structure, and meanwhile reduce the valance state of Ni to introduce Ni^{2+} orbital configurates, e.g., Ni^{3+}/Ni^{2+}=(n-1)/1 [20]. As a result, an electron more localized

* Corresponding author.
E-mail address: jikunchen@ustb.edu.cn (J. Chen).

https://doi.org/10.1016/j.scriptamat.2025.116720
Received 4 December 2024; Received in revised form 9 April 2025; Accepted 17 April 2025
Available online 21 April 2025

phase is expected for reducing n from infinitely large (e.g., $ReNiO_3$) towards 1 (e.g., Re_2NiO_4), and this sheds a light on the emergency of additional MIT behaviors for $Re_{n+1}Ni_nO_{3n+1}$ with n in between. This understanding was previously well supported in the more abrupt MIT behavior of $La_3Ni_2O_7$ at a relatively high T_{MIT} at 560 K compared to $ReNiO_3$ with heavy rare-earth compositions [15], while $La_4Ni_3O_{10}$ and La_2NiO_4 are in metallic and insulating phase, respectively, across an entire range of temperature [21–23]. Nevertheless, whether it is possible to further adjust the T_{MIT} of $Re_3Ni_2O_7$ yet remains as an open question to be explored, since a continuously adjustable MIT is vital for high-temperature applications.

In this work, we demonstrate more abrupt MIT behaviors with continuously adjustable T_{MIT} within high temperature range of 500–560 K in the layered perovskite nickelates $La_{3-x}Bi_xNi_2O_7$, compared to the $ReNiO_3$ exhibiting similar T_{MIT}. The regulation in lattice constants and electronic structures via Bi substitution of $La_3Ni_2O_7$ were investigated by structural refinement of their X-ray diffraction (XRD) patterns and synchrotron based near edge X-ray absorption fine structure analysis (NEXAFS), respectively. The respective adjustment in their electrical transportation properties were characterized within a temperature range of 5–300 K and further fitted by using the nearest-neighbors hopping model, while the presence of an anomalous transition in the type of carriers was indicated by the thermopower of $La_{3-x}Bi_xNi_2O_7$. In addition to achieving a larger resistive switch at high T_{MIT} compared to $ReNiO_3$ with middle or heavy rare-earth composition, we also highlight the higher material stability in both air and Ar atmosphere up to 1130 °C and 1000 °C, respectively, paving the way to their applications in higher temperature ranges.

We synthesized a series of $La_{3-x}Bi_xNi_2O_7$, $La_{3-x}Pr_xNi_2O_7$ and $La_{3-x}Nd_xNi_2O_7$ with x ranging from 0.025 to 0.3 via conventional solid-state reaction in air at 1100 °C. Fig. 1a demonstrates a representative XRD pattern for as-made $La_{2.95}Bi_{0.05}Ni_2O_7$, while more of their respective XRD patterns for $La_{3-x}Bi_xNi_2O_7$ are shown in Figure S1. At a low Bi substitution ratio (e.g., $x < 0.1$), as-synthesized powder exhibits a layered perovskite structure similar to $La_3Ni_2O_7$ without the observation of obvious impurity phases. The crystal structure of such 327-type Ruddlesden-Popper layered perovskite is further illustrated in the inset of Fig. 1a, where a single rock-salt layer (e.g., LaO) are alternatively stacked with two layers of perovskite structure ($LaNiO_3$). As synthesized powders are in rectangular shape at micrometer size, as demonstrated by their representative SEM morphologies shown in Fig. 1b.

The lattice parameters of as-synthesized $La_{3-x}Bi_xNi_2O_7$, La_{3-x}

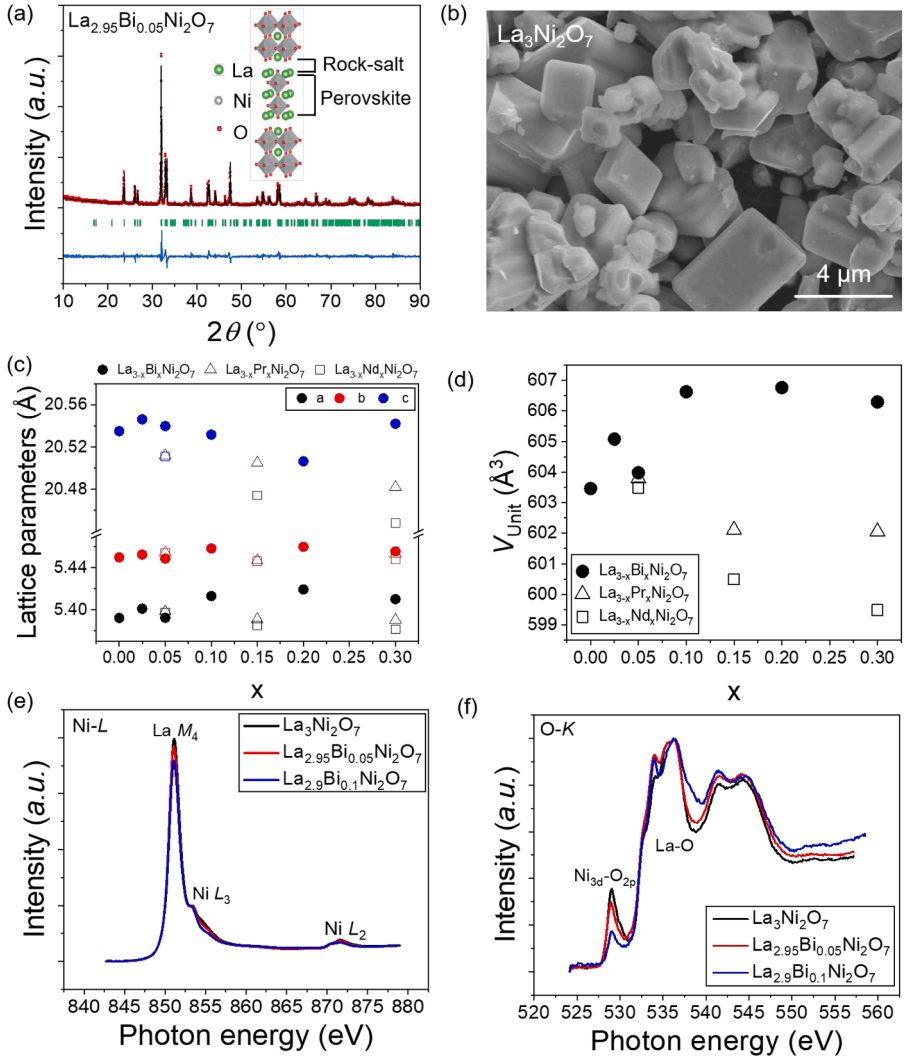

Fig. 1. (a) The XRD patterns for $La_{2.95}Bi_{0.05}Ni_2O_7$ (circles) together with its fitting results via XRD Rietveld refinement (full line). (b) The scanning electron microscopy (SEM) micrographs for $La_3Ni_2O_7$. (c) The respective lattice parameters (a, b, c) and (d) the volume of unit cell (V_{Unit}) plotted as a function of the ratio in the lighter rare-earth substitution (x) for the $La_{3-x}Bi_xNi_2O_7$ ($x = 0$, 0.025, 0.05, 0.1, 0.2, 0.3), $La_{3-x}Pr_xNi_2O_7$ ($x = 0.05$, 0.15, 0.3), and $La_{3-x}Nd_xNi_2O_7$ ($x = 0.05$, 0.15, 0.3). The near-edge X-ray absorption fine structure (NEXAFS) analysis for (e) the Ni-*L* edge and (f) the O-*K* edge as measured for the nominally synthesized powder of $La_{3-x}Bi_xNi_2O_7$($x = 0$, 0.05, 0.1).

$_xNd_xNi_2O_7$ and $La_{3-x}Pr_xNi_2O_7$ were determined from Rietveld refinement of their XRD patterns (see more details in Figure S1 and Figure S2) as plotted in Fig. 1c as a function of *x*, and this is further compared to substituting the La-site by conventional rare-earth elements (e.g., Pr and Nd). It can be seen that the Bi substitution of La results in slight expansions in *a* and *b*, while *c* shows a nonmonotonic tendency, e.g., firstly expands for increasing x to 0.025 and afterwards slightly decreases. This is in contrast to the tendencies for substituting the La-site by smaller rare-earths such as Pr or Nd, in which situations more monotonic shrinkages are observed with an increasing *x*. In Fig. 1d, a nonmonotonic tendency is observed for $La_{3-x}Bi_xNi_2O_7$ as their unit cell expands rapidly when enlarging x until 0.025 and afterwards shrinks a bit. In contrast, the unit cell for $La_{3-x}Pr_xNi_2O_7$ and $La_{3-x}Nd_xNi_2O_7$ shrinks monotonically with an increasing *x*. It indicates the distinct regulation in structures via Bi substitution of the La compared to the common rare-earth substitution, in which case the unit cells of $La_{3-x}Bi_xNi_2O_7$ do not simply expand via substituting La^{3+} with the larger and more covalent Bi^{3+}.

To further investigate the respective regulation in electronic structures, the Ni-L and O-*K* edges of $La_{3-x}Bi_xNi_2O_7$ were probed by the near edge X-ray absorption fine structure (NEXAFS) analysis, as demonstrated in Fig. 1e and 1f, respectively. The Ni-*L* edge originates from electron transition from 3d to 2p, while the O-*K* edge reflects Ni_{3d}-O_{2p} hybridization and *Re*-O coupling [24]. Compared to *Re*NiO_3 and NiO, $La_3Ni_2O_7$ has predominant $3d^8\underline{L}$ occupation state, with expanded satellite peak at the Ni-*L* edge and high pre-peak at O-*K* edge [25]. Comparing the Ni-*L* edge NEXAFS spectrum as shown in Fig. 1f, a decreasing tendency in the peaks at the Ni-L_3 and Ni-L_2 energies is clearly observed with an increasing of Bi doping ratio. Comparing the O-*K* edge NEXAFS spectra of $La_{2.95}Bi_{0.05}Ni_2O_7$ and $La_{2.9}Bi_{0.1}Ni_2O_7$ to that of $La_3Ni_2O_7$ shown in Fig. 1e, we can clearly see that the main effect is the reduction in the pre-peak height in the spectrum for $La_{3-x}Bi_xNi_2O_7$ with an increasing x. It suggests that oxygen vacancies are gradually decrease and the ground state is closer to $\alpha|3d^8\rangle+\beta|3d^9\underline{L}\rangle$ [25].

These observations indicate the reduction in Ni^{3+} configuration compared to Ni^{2+} when substitute the La-site by Bi in $La_{3-x}Bi_xNi_2O_7$. It also demonstrates the difference for the present Bi substitution compared to conventional rare-earth substitutions for perovskite nickelates [11,26]. Usually, rare-earth substitution via the ones with larger ionc radius should straighten the Ni-O-Ni bond angle and strengthen the Ni^{3+} configuration compared to the Ni^{2+} in *Re*NiO_3, but this is not the present case although the Bi^{3+} is larger than La^{3+}. Compared to conventional rare-earth ions that mainly determines the relative distortion of the NiO_6 octahedra, the Bi^{3+} is more covalent and can more directly participate to the formation of the conduction and/or valance bands. The orbital interaction associated with Bi-O compete with and weakens the one associated with the previous Ni-O, and therefore descend the valance of Ni.

Fig. 2a demonstrates the temperature dependence of the material resistivity (ρ-*T*) for $La_{3-x}Bi_xNi_2O_7$ with various Bi substitution composition (x), while the ρ-*T* tendencies for $La_{3-x}Nd_xNi_2O_7$ and $La_{3-x}Pr_xNi_2O_7$ are demonstrated in Figure S3. In general, a weak insulating (or bad metal) ρ-*T* tendency was observed below T_{MIT}, while further elevating the temperature results in metallic transportation behavior as more clearly demonstrated in Figure S4. The magnitude of T_{MIT} as further shown in Figure S5, respectively for $La_{3-x}Bi_xNi_2O_7$ and $La_{3-x}Nd_xNi_2O_7$ ($La_{3-x}Pr_xNi_2O_7$). It can be seen that the T_{MIT} of $La_{3-x}Bi_xNi_2O_7$ effectively descends from 560 K to 500 K when increasing x up to 0.3. Afterwards, the T_{MIT} remains constant by further increasing x (e.g., up to 0.4), as more clearly demonstrated in the inset of Fig. 2a. In contrast, no obvious regulations in the T_{MIT} are observed in $La_{3-x}Nd_xNi_2O_7$ and $La_{3-x}Pr_xNi_2O_7$, compared to $La_3Ni_2O_7$.

To confirm the role of Bi substitution in the regulation of T_{MIT}, instead of potentially varying the oxygen composition (or generating vacancy), we annealed representative samples of $La_{3-x}Bi_xNi_2O_7$ ($x = 0$, 0.04, 0.1) in 10 MPa-high oxygen pressures at 800 °C for 24 h. As their XRD patterns shown in Figure S6, the high-oxygen pressure annealed $La_3Ni_2O_7$ and $La_{2.96}Bi_{0.04}Ni_2O_7$ maintains the pristine 327-typed layered perovskite structure, with a slightly rightwards shift in their diffraction peaks indicating the shrinkage in lattice constants. In contrast, further increasing x (e.g., up to 0.1) varies their crystal structure towards a more stable 214-type layered perovskite structure. Figure S7 compares the ρ-*T* tendency of $La_{3-x}Bi_xNi_2O_7$ ($x = 0$, 0.04, 0.1) before and after the high oxygen pressure anneals, and it can be seen that compensating the oxygen vacancy via high pressure oxygen anneals reduces the material resistivity. However, the T_{MIT} of $La_3Ni_2O_7$ remained stable while that of $La_{2.96}Bi_{0.04}Ni_2O_7$ slightly descends.

In Fig. 2b, the resistive switch ($\rho_{Insul.}/\rho_{Met.}$) across T_{MIT} are compared for as-synthesized $La_{3-x}Bi_xNi_2O_7$ to the ones for the 113-type perovskite nickelates. It demonstrates the more abrupt MIT property as achieved in $La_{3-x}Bi_xNi_2O_7$ compared to the *Re*NiO_3 with middle or heavy composition showing similar T_{MIT} [11,27–29]. It is also interesting to note the nonmonotonic tendency in the resistive change of $La_{3-x}Bi_xNi_2O_7$ with an increasing x, as more clearly shown in the inset of Fig. 2b. Differs to the situation of Bi substitution, the changes in $\rho_{Insul.}/\rho_{Met.}$ are not significant when substituting the La-site with other rare-earth (e.g., Pr and Nd) as demonstrated in Fig. 2b (see more details in Figure S8 and Figure S9).

The ρ-*T* tendencies of as-grown $La_{3-x}Bi_xNi_2O_7$, $La_{3-x}Nd_xNi_2O_7$ and $La_{3-x}Pr_xNi_2O_7$ were also characterized at the low temperature range, as shown in Fig. 3a. It is interesting to note that the $La_3Ni_2O_7$ or substituted $La_3Ni_2O_7$ exhibits a smaller temperature dependence below T_{MIT}, compared to the insulating (or semiconductive) phase of *Re*NiO_3.

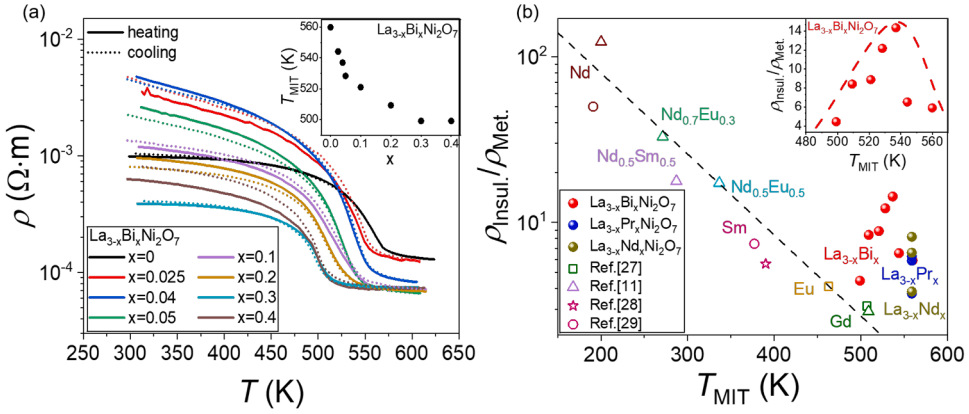

Fig. 2. (a) The temperature dependent resistivity as measured for $La_{3-x}Bi_xNi_2O_7$($x = 0$, 0.025, 0.04, 0.05, 0.1, 0.2, 0.3, 0.4) in air atmosphere via both process of heating up (full line) and cooling down (broken line). (b) The variation in material resistivity across T_{MIT}, ($\rho_{Insul.}/\rho_{Met.}$), plotted as a function of T_{MIT} for the samples made in our work and the previous reports [11,27–29].

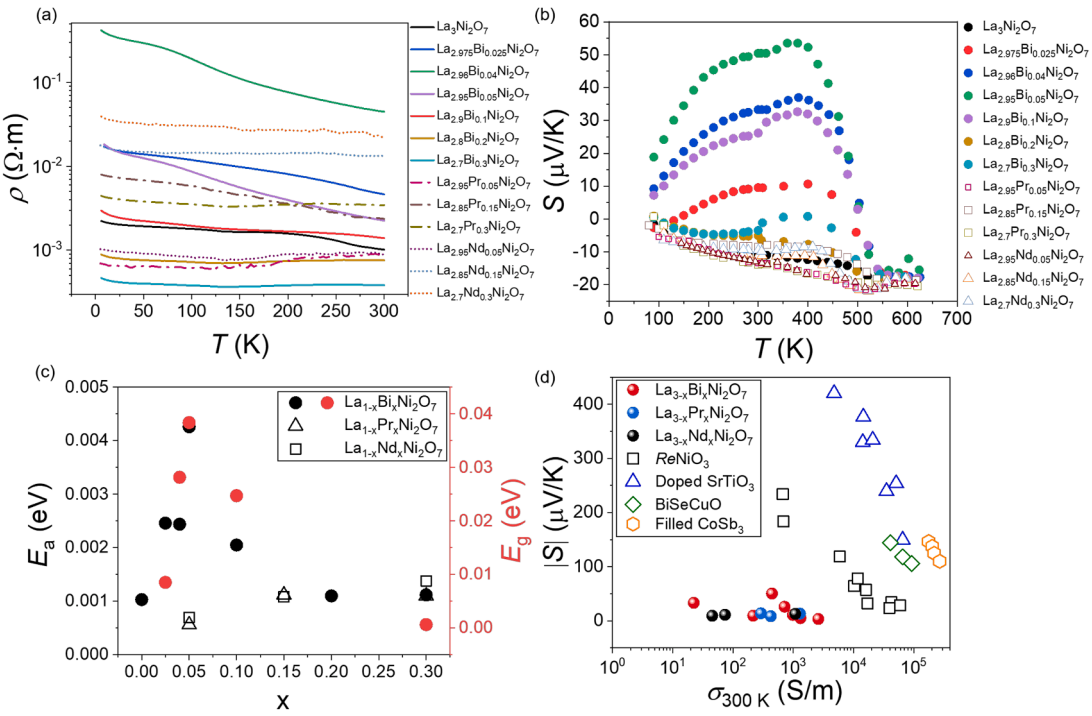

Fig. 3. (a) The temperature dependent resistivity as measured for the $La_{3-x}Bi_xNi_2O_7$ ($x = 0$, 0.025,0.04,0.05, 0.1,0.2,0.3), $La_{3-x}Pr_xNi_2O_7$($x = 0.05$, 0.15, 0.3), and $La_{3-x}Nd_xNi_2O_7$ ($x = 0.05$, 0.15, 0.3) sintered in air atmosphere. (b) The temperature dependent Seebeck coefficient as measured for $La_{3-x}Bi_xNi_2O_7$($x = 0$, 0.025,0.04,0.05, 0.1,0.2,0.3,0.4) in air atmosphere. (c) The derived activation energy of carrier hopping for the $La_{3-x}Bi_xNi_2O_7$($x = 0$, 0.025, 0.04, 0.05, 0.1, 0.2, 0.3), $La_{3-x}Pr_xNi_2O_7$ ($x = 0.05$, 0.15, 0.3) and $La_{3-x}Nd_xNi_2O_7$ ($x = 0.05$, 0.15, 0.3) and the energy band gap of the $La_{3-x}Bi_xNi_2O_7$($x = 0.025$, 0.04, 0.05, 0.1, 0.3). (d) The S-σ (σ: electrical conductivity) for the $La_{3-x}Bi_xNi_2O_7$($x = 0$, 0.025, 0.04, 0.05, 0.1, 0.2, 0.3), $La_{3-x}Pr_xNi_2O_7$ ($x = 0.05$, 0.15, 0.3) and $La_{3-x}Nd_xNi_2O_7$ ($x = 0.05$, 0.15, 0.3) samples in this work with conventional thermoelectric compounds, such as *Re*NiO_3 [31], doped $SrTiO_3$ [32–34], BiSeCuO [35], and filled $CoSb_3$ [36].

Substituting the La with Nd or Pr elevates the ground state resistivity, while Bi substitution of La firstly elevates the resistivity of $La_{3-x}Bi_xNi_2O_7$ (e.g., up to $x = 0.04$) and afterwards reduces the resistivity.

In Fig. 3b, the temperature dependences of the thermopower (S-T) are compared for $La_{3-x}Bi_xNi_2O_7$, $La_{3-x}Nd_xNi_2O_7$ and $La_{3-x}Pr_xNi_2O_7$. It can be seen that the $La_3Ni_2O_7$ exhibits a relatively small thermopower with negative magnitudes indicating its transportation as dominated by electrons, while no significant variations in the S-T tendency are observed when substituting La by Nd or Pr. In contrast, substituting La by Bi results in nonmonotonic adjustment in the thermopower of $La_{3-x}Bi_xNi_2O_7$ with x, towards the positive magnitude and maximized at $x = 0.05$. This indicates that the type of major carrier corresponding for the electrical conductance was switched from the previous electrons towards the holes.

From the ρ-T and S-T tendencies, the activation energy (E_a) associated with the carrier transportation as well as the energy band gap (E_g) were further calculated. In brief, from the slope of the ln ($\rho_T/\rho_{50\ K}$)-1000/T tendency, the E_a can be further derived as plotted in Figure S10. The magnitudes of the Seebeck coefficient has a maximum value ($|S|_{max}$) at specific temperature (T_{max}) and can be used to estimate their energy band gap (E_g) under nondegenerate approximation, as E_g=2e$T_{max}|S|_{max}$ [30]. In Fig. 3c, it can be seen that both E_a and E_g experience non-monotonic variations when substituting the La-site with Bi, e.g., their peak magnitudes appear at $x = 0.05$. This differs to the situations when performing conventional rare-earth substitutions for the *Re*NiO_3, in which cases E_a is monotonically increasing when reducing the rare-earth radius (e.g., substituting La by Nd or Pr).

In Fig. 3d, the thermopower of $La_{3-x}Bi_xNi_2O_7$, $La_{3-x}Nd_xNi_2O_7$ and $La_{3-x}Pr_xNi_2O_7$ measured at room temperature are plotted as a function of their respective electrical conductivity, and this is further compared with *Re*NiO_3 as well as other representative oxide semiconductors [31–36]. It can be seen that in general, the magnitude is the $|S|$ of nickelates is smaller compared to conventional semiconductors at similar magnitude of electronical conductance. In particular, compared to the *Re*NiO_3, the 327-type layered perovskite nickelates exhibits much smaller thermopower that is nearly not dependent to their electrical conductivity. It unveils that both electrons and holes may contribute for the major carrier transportation in these 327-type layered perovskite nickelates. Considering the NEXAFS results shown in Fig. 1e and 1f, the weakening in Ni-O orbital interaction via effective Bi substitution is expected to arouse more localized electron transportations within $La_{3-x}Bi_xNi_2O_7$, and this elevates the hole contribution to the transportations and alters the thermopower towards the positive magnitude.

Apart from the above distinguished electronic feature and regulatable MIT behaviors associated with $La_{3-x}Bi_xNi_2O_7$, their material stability is also important to potential device applications. The material stability of $La_{3-x}Bi_xNi_2O_7$ is further investigated by performing thermogravimetric analysis (TGA), as shown in Fig. 4a. It can be seen that the $La_3Ni_2O_7$ exhibits a high decomposition temperature of ~1230 °C in air and ~1050 °C in argon, while the decomposition temperature was slightly reduced via Bi substitution (e.g., ~1130 °C in air and ~1000 °C in argon for $La_{2.9}Bi_{0.1}Ni_2O_7$) but still largely exceed the ones for *Re*NiO_3 (e.g., ~900 °C for $SmNiO_3$ in air [37]). As the representative XRD patterns of the air annealed samples shown in Fig. 4b, the $La_{2.9}Bi_{0.1}Ni_2O_7$ annealed at 1100 °C well preserve its pristine crystal structure, while further elevation in the annealing temperature varies their crystal structure towards a more stable 214-type layered structure.

In summary, we show adjustable MIT properties in $La_{3-x}Bi_xNi_2O_7$ with T_{MIT} from 500 to 560 K, featuring a more abrupt resistive switch than previous *Re*NiO_3 with middle or heavy rare-earth compositions. The Bi substitution up to $x = 0.3$ results in effective lattice expansion and relieves the distortion in the NiO_6 octahedra of $La_{3-x}Bi_xNi_2O_7$, as indicated by XRD refinement. Nevertheless, the Bi substitution strengthens the electron localized Ni^{2+} configuration compared to the electron itinerant Ni^{3+} within $La_{3-x}Bi_xNi_2O_7$ as demonstrated by NEXAFS, owing to the more covalent nature of Bi^{3+} that compete bonding with oxygen.

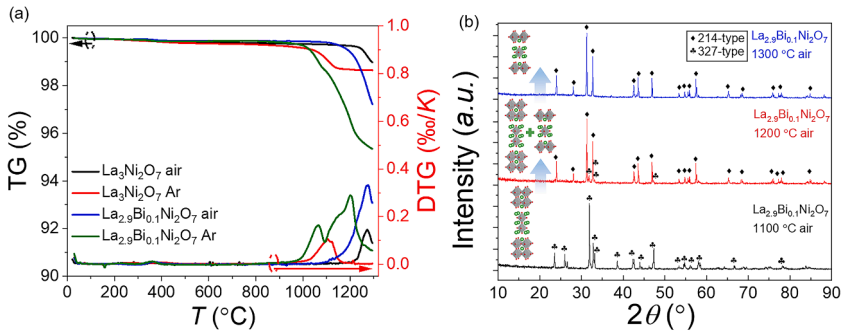

Fig. 4. (a) Thermogravimetry and derivative thermogravimetry (TG-DTG) curve of $La_3Ni_2O_7$ and $La_{2.9}Bi_{0.1}Ni_2O_7$ powder in air and argon. (d) The XRD patterns of the $La_{2.9}Bi_{0.1}Ni_2O_7$ ceramics sintered in air atmosphere.

It is also worth noticing anomalously small magnitudes in the thermopowers of the insulating $La_{3-x}Bi_xNi_2O_7$, compared to the one observed in *Re*NiO_3 at similar electrical conductivity. This indicates the distinguished bi-polar transport characters for $La_3Ni_2O_7$, while the Bi substitution results in electron localization and thereby elevates the hole contribution to the transportation to drive the thermopower of their insulating phase towards the positive magnitude. A nonmonotonic variation in the abruption of MIT was observed for varying the Bi-substitution ratio, while a large $\rho_{Insul.}/\rho_{Met.}$ ratio exceeding one order of magnitude was achieved at high T_{MIT} above 540 K for $La_{2.96}Bi_{0.04}Ni_2O_7$. Compared to the *Re*$NiO_3$ with similar high T_{MIT}, the $La_{3-x}Bi_xNi_2O_7$ exhibits higher material stability up to 1130 °C and 1000 °C in air and Ar atmospheres, respectively, paving the way to their potential applications at high temperature ranges.

Availability of data

The data that support the findings of this study are available from the corresponding author upon reasonable request.

CRediT authorship contribution statement

Hao Zhang: Writing – review & editing, Writing – original draft, Methodology, Formal analysis, Data curation. **Jingxin Gao:** Writing – review & editing, Methodology, Data curation. **Yi Bian:** Writing – review & editing, Methodology, Data curation. **Wei Lei:** Writing – review & editing, Formal analysis. **Hongliang Dong:** Writing – review & editing, Supervision, Methodology, Conceptualization. **Xiaoguang Xu:** Writing – review & editing, Supervision, Conceptualization. **Nuofu Chen:** Writing – review & editing, Methodology, Conceptualization. **Jikun Chen:** Writing – review & editing, Writing – original draft, Funding acquisition, Formal analysis, Conceptualization.

Declaration of competing interest

The authors declare that they have no known competing financial interests or personal relationships that could have appeared to influence the work reported in this paper.

Acknowledgements

This work was supported by the National Key Research and Development Program of China (No. 2021YFA0718900), the National Natural Science Foundation of China (No. 62474017 and 52073090). J. Chen also acknowledge Xiaomi Scholar project. The authors also acknowledge the financial support from Shanghai Key Laboratory of Material Frontiers Research in Extreme Environments (MFree), China (No. 22dz2260800) and Shanghai Science and Technology Committee, China (No. 22JC1410300). We also thank the 4B9B beamline station at Beijing Synchrotron Radiation Facility (BSRF) for the help in characterizations.

Supplementary materials

Supplementary material associated with this article can be found, in the online version, at doi:10.1016/j.scriptamat.2025.116720.

References

[1] M.María Luisa, Structural, magnetic and electronic properties of $RNiO_3$ perovskites (R = rare earth), J. Phys. Condens. Matter 9 (1997) 1679.
[2] F. Conchon, A. Boulle, R. Guinebretière, C. Girardot, S. Pignard, J. Kreisel, F. Weiss, E. Dooryhée, J.L. Hodeau, Effect of tensile and compressive strains on the transport properties of $SmNiO_3$ layers epitaxially grown on (001) $SrTiO_3$ and $LaAlO_3$ substrates, Appl. Phys. Lett. 91 (2007) 192110.
[3] J. Li, S. Ramanathan, R. Comin, Carrier Doping Physics of Rare Earth Perovskite Nickelates *RE*NiO_3, Front. Phys. 10 (2022) 834882.
[4] Z. Li, F. Yan, X. Li, Y. Cui, V. Wang, J. Wang, C. Liu, Y. Jiang, N. Chen, J. Chen, Molten-salt synthesis of rare-earth nickelate electronic transition semiconductors at medium high metastability, Scr. Mater. 207 (2022) 114271.
[5] A. Feteira, Negative temperature coefficient resistance (NTCR) Ceramic thermistors: an industrial perspective, J. Am. Ceram. Soc. 92 (2009) 967–983.
[6] H.T. Zhang, T.J. Park, A.N.M.N. Islam, D.S.J. Tran, S. Manna, Q. Wang, S. Mondal, H. Yu, S. Banik, S. Cheng, H. Zhou, S. Gamage, S. Mahapatra, Y. Zhu, Y. Abate, N. Jiang, S.K.R.S. Sankaranarayanan, A. Sengupta, C. Teuscher, S. Ramanathan, Reconfigurable perovskite nickelate electronics for artificial intelligence, Science 375 (2022) 533–539.
[7] J. Shi, S.D. Ha, Y. Zhou, F. Schoofs, S. Ramanathan, A correlated nickelate synaptic transistor, Nat. Commun. 4 (2013) 2676.
[8] A. Shahsafi, P. Roney, Y. Zhou, Z. Zhang, Y. Xiao, C. Wan, R. Wambold, J. Salman, Z. Yu, J. Li, J.T. Sadowski, R. Comin, S. Ramanathan, M.A. Kats, Temperature-independent thermal radiation, Proc. Natl. Acad. Sci. 116 (2019) 26402–26406.
[9] G. Catalan, Progress in perovskite nickelate research, Phase Trans. 81 (2008) 729–749.
[10] X. Li, T. Zhang, Z. Li, F. Yan, H. Li, Y. Cui, N. Chen, J. Chen, Nonlinearity in regulating the metal to insulator transition of *Re*NiO_3 towards low temperature range, Ceram. Int. 48 (2022) 31995–32000.
[11] J. Zhong, Z. Li, Y. Zheng, P. Jiang, F. Zhang, T. Zhang, Y. Cui, Z. Zhong, N. Chen, J. Chen, Extending the metal to insulator transitions of rare-earth nickelates towards low temperature ranges, J. Am. Ceram. Soc. 106 (2023) 5067–5077.
[12] I.V. Nikulin, M.A. Novojilov, A.R. Kaul, A.F. Maiorova, S.N. Mudretsova, Synthesis and transport properties study of $Nd_{1-x}Sm_xNiO_{3-\delta}$ solid solutions, Mater. Res. Bull. 39 (2004) 803–810.
[13] Z. Zhang, D. Schwanz, B. Narayanan, M. Kotiuga, J.A. Dura, M. Cherukara, H. Zhou, J.W. Freeland, J. Li, R. Sutarto, F. He, C. Wu, J. Zhu, Y. Sun, K. Ramadoss, S.S. Nonnenmann, N. Yu, R. Comin, K.M. Rabe, S.K.R.S. Sankaranarayanan, S. Ramanathan, Perovskite nickelates as electric-field sensors in salt water, Nature 553 (2017) 68–72.
[14] J. Chen, H. Hu, J. Wang, T. Yajima, B. Ge, X. Ke, H. Dong, Y. Jiang, N. Chen, Overcoming synthetic metastabilities and revealing metal-to-insulator transition & thermistor bi-functionalities for D-band correlation perovskite nickelates, Mater. Horiz. 6 (2019) 788–795.
[15] W. Singkha, S. Kuharuangrong, Electrical Property of Mn and Co Dopants on $La_3Ni_2O_{7\pm\delta}$ and $La_{2.9}Sr_{0.1}Ni_2O_{7\pm\delta}$, Adv. Mater. Res. 93-94 (2010) 566–569.
[16] S. Kuharuangrong, N. Ratchasima Synthesis and Physical Properties of $La_{3-x}Sr_xNi_2O_{7\pm\delta}$ Ruddlesden-Popper Phase, J. Met. Mater. Miner. 18 (2008) 77.
[17] Y. Adachi, N. Hatada, K. Hirota, M. Kato, T. Uda, Preparation of pure and fully dense lanthanum nickelates $La_{n+1}Ni_nO_{3n+1}$ (n = 2, 3, ∞) by post-sintering oxidation process, J. Am. Ceram. Soc. 102 (2019) 7077–7088.
[18] C.D. Ling, D.N. Argyriou, G. Wu, J.J. Neumeier, Neutron Diffraction Study of $La_3Ni_2O_7$: structural Relationships Among n=1, 2, and 3 Phases $La_{n+1}Ni_nO_{3n+1}$, J. Solid State Chem. 152 (2000) 517–525.
[19] S.A. Nedilko, V.A. Kulichenko, A.G. Dziazko, E.G. Zenkovich, Oxygen nonstoichiometry and properties of lanthanum nickelates $La_{3-x}Ca_xNi_2O_{7-\delta}$ ($0 \le x \le 2.0$), J. Alloys Compd. 367 (2004) 251–254.

[20] F. Gervais, P. Odier, Y. Nigara, Plasmon behavior at the “semiconductor-metal” transition in La_2NiO_4 and $La_3Ni_2O_7$, Solid State Commun 56 (1985) 371–374.
[21] S. Huangfu, X. Zhang, A. Schilling, Correlation between the tolerance factor and phase transition in $A_{4-x}B_xNi_3O_{10}$(A and B=La,Pr,and Nd; x=0,1,2, and 3), Phys. Rev. Res. 2 (2020) 033247.
[22] K. Ishikawa, S.-i. Kondo, Y. Suzuki, S.-i. Takayama, K. Shimada, Y. Suzuki, The Electrical Properties of $La_{2-x}Sr_xNiO_4$ ($0\leq x\leq 1$), Bull. Chem. Soc. Jpn. 59 (2006) 703–706.
[23] Z. Zhang, M. Greenblatt, Synthesis, Structure, and Properties of $Ln_4Ni_3O_{10-\delta}$ (Ln = La, Pr, and Nd), J. Solid State Chem. 117 (1995) 236–246.
[24] J.W. Freeland, M. van Veenendaal, J. Chakhalian, Evolution of electronic structure across the rare-earth $RNiO_3$ series, J. Electron. Spectrosc. Relat. Phenom. 208 (2016) 56–62.
[25] X. Chen, J. Choi, Z. Jiang, J. Mei, K. Jiang, J. Li, S. Agrestini, M. Garcia-Fernandez, H. Sun, X. Huang, D. Shen, M. Wang, J. Hu, Y. Lu, K.-J. Zhou, D. Feng, Electronic and magnetic excitations in $La_3Ni_2O_7$, Nat. Commun. 15 (2024) 9597.
[26] F. Yan, Z. Li, H. Zhang, Y. Cui, K. Nie, N. Chen, J. Chen, Temperature-sensing array using the metal-to-insulator transition of $Nd_xSm_{1-x}NiO_3$, Miner, Metall. Mater. 31 (2024) 1694–1700.
[27] H. Zhang, Y. Bian, Y. Xia, Y. Cui, Z. Li, F. Zhang, Y. Bai, N. Chen, J. Chen, Correlated perovskite nickelates with valence variable rare-earth compositions, J. Rare Earths 42 (2024) 743–748.
[28] M.T. Escote, A.M.L. da Silva, J.R. Matos, R.F. Jardim, General Properties of Polycrystalline $LnNiO_3$ (Ln=Pr, Nd, Sm) Compounds Prepared through Different Precursors, J. Solid State Chem. 151 (2000) 298–307.
[29] I.V. Nikulin, M.A. Novojilov, A.R. Kaul, S.N. Mudretsova, S.V. Kondrashov, Oxygen nonstoichiometry of $NdNiO_{3-\delta}$ and $SmNiO_{3-\delta}$, Mater. Res. Bull. 39 (2004) 775–791.
[30] H.J. Goldsmid, J.W. Sharp, Estimation of the thermal band gap of a semiconductor from seebeck measurements, J. Electron. Mater. 28 (1999) 869–872.
[31] J. Chen, H. Hu, J. Wang, C. Liu, X. Liu, Z. Li, N. Chen, A D-Band electron correlated thermoelectric thermistor established in metastable perovskite family of rare-earth nickelates, ACS Appl. Mater. Interfaces 11 (2019) 34128–34134.
[32] H. Ohta, K. Sugiura, K. Koumoto, Recent progress in oxide thermoelectric materials: p-type $Ca_3Co_4O_9$ and n-type $SrTiO_3$, Inorg. Chem. 47 (2008) 8429–8436.
[33] T. Okuda, K. Nakanishi, S. Miyasaka, Y. Tokura, Large thermoelectric response of metallic perovskites:$Sr_{1-x}LaxTiO_3$ ($0\leq x\leq 0.1$), Phys. Rev. B 63 (2001) 113104.
[34] A.I. Abutaha, S.R. Sarath Kumar, H.N. Alshareef, Laser energy tuning of carrier effective mass and thermopower in epitaxial oxide thin films, Appl. Phys. Lett. 100 (2012) 162106.
[35] R. Liu, X. Tan, Y. Liu, G. Ren, J.l. Lan, Z. Zhou, C. Nan, Y. Lin, BiCuSeO as state-of-the-art thermoelectric materials for energy conversion: from thin films to bulks, Rare Met 37 (2018) 259–273.
[36] Z. Xiong, X. Chen, X. Huang, S. Bai, L. Chen, High thermoelectric performance of $Yb_{0.26}Co_4Sb_{12}/y$GaSb nanocomposites originating from scattering electrons of low energy, Acta Mater 58 (2010) 3995–4002.
[37] H. Zhang, Z. Li, T. Zhang, Y. Cui, S. Du, J. Zhong, L. Meng, N. Chen, J. Chen, Improvement of metal–insulator transition and mechanical strength of $RENiO_3$ by co-sintering, J. Appl. Phys. 134 (2023) 135104.